

The Ocean One hands: An adaptive design for robust marine manipulation

The International Journal of
Robotics Research
2017, Vol. 36(2) 150–166
© The Author(s) 2017
Reprints and permissions:
sagepub.co.uk/journalsPermissions.nav
DOI: 10.1177/0278364917694723
journals.sagepub.com/home/ijr



Hannah Stuart¹, Shiquan Wang¹, Oussama Khatib² and Mark R Cutkosky¹

Abstract

Underactuated, compliant, tendon-driven robotic hands are suited for deep-sea exploration. The robust Ocean One hand design utilizes elastic finger joints and a spring transmission to achieve a variety of pinch and wrap grasps. Compliance in the fingers and transmission determines the degree of load-sharing among contacts and the hands' ability to secure irregularly shaped objects. However, it can also decrease external grasp stiffness and acquisition reliability. SimGrasp, a flexible dynamic hand simulator, enables parametric studies of the hand for acquisition and pull-out tests with varying transmission spring rates. In the present application, we take advantage of achieving different stiffnesses by reversing the direction of tendon windup using a torsional spring-loaded winch. With this provision, the hand can be relatively soft for handling delicate objects and stiff for tasks requiring strength. Two hands were field-tested as part of the Ocean One humanoid platform, which acquired a vase from the La Lune shipwreck site at a 91 m depth in the Mediterranean Sea.

Keywords

Multifingered hands, marine robotics, grasping, underactuated robots, mechanism design, field robots

1. Introduction

Underactuation is a robust and adaptable solution for grasping and manipulation in unstructured environments. Compliant, underactuated hands can perform capably with simple control, often using compact, lightweight and resilient load-sharing mechanisms. As a consequence, they have been proposed widely for mobile robotic and prosthetic applications. In each case, however, the design of the hand involves trade-offs concerning the number of fingers and actuators (e.g. one motor per finger or one motor for the entire hand) and the amount of compliance in the fingers and transmission. As a result, each underactuated hand is somewhat specialized for a range of tasks.

In the present case, the application is undersea exploration using the Ocean One platform (Khatib et al., 2016). Tasks include acquiring and manipulating large and small objects with one or two hands. Objects range from small and delicate pieces of coral to heavy frames and tools. They can also be slippery; the coefficient of friction in silty seawater is typically lower than in air, and objects may be covered in slimy biofilm. In some cases objects can be partially trapped, so the hand may need the ability to pull with large forces. The hands are also used for temporarily anchoring the robot against ocean currents. Finally, because the Ocean One robot is conspicuously humanoid – intended as an avatar for scientists controlling it from a boat – the hands benefit from being relatively anthropomorphic (Figure 1).

Section 2 reviews related prior work on under actuated hands, focusing on those most relevant to the problem of designing hands that can acquire and secure a variety of large and small objects in uncertain conditions. Section 3 then introduces the design of the hands, including the overall configuration, the compliant tendon-driven fingers, and the transmission system with torsional springs, which allows the operator to select grasp stiffness with actuation direction. Because the selection of compliances in the transmission and fingers necessarily involves trade-offs, Section 4 provides an analysis of the overall stiffness for object grasping and acquisition tasks. We first present a simplified planar example to illustrate the main points. Then we present the results of numerical simulations and experiments in Section 5 to confirm the predicted trends. We find it is important to provide both soft and stiff grasping modes to a teleoperator in order to satisfy requirements for ocean exploration. This work may inform operator selection of grasp stiffness, considering both object shape and external force direction. Finally, Section 6 reports on

¹Department of Mechanical Engineering, Stanford University, USA

²Department of Computer Science, Stanford University, USA

Corresponding author:

Hannah Stuart, Biomimetic and Dexterous Manipulation Lab, 418 Panama Mall, Bldg 02-660 Rm 132, Stanford, CA, 94305, USA.
Email: hstuart@stanford.edu



Fig. 1. *Ocean One* diving in the Mediterranean for its first mission, which included investigating a shipwreck off the coast of Toulon, France. Photo credit: Frederic Osada and Teddy Seguin/DRASSM/Stanford University.

field demonstrations of the hand through a mission with the French Département des Recherches Archéologiques Subaquatiques et Sous-Marines (DRASSM) to explore a shipwreck off the coast of Toulon, France.

2. Related prior work

Underactuated adaptive fingers and transmissions can simplify grasping by load-sharing passively among combinations of phalanges and fingers. Typically, adaptability also increases impact resilience and the ability to conform to irregular surfaces, albeit at the expense of manipulation precision. Underactuated hands are also typically less complex than fully actuated hands, which tend to be bulky, challenging to control, and usually require more sensors. Consequently, underactuated hands are often a good choice for robots in unstructured environments and prosthetics. As noted by Birglen et al. (2008), examples can be found as early as Pringle's 1919 patent (Pringle, 1919). Since then, a large literature has developed concerning the design, modeling and control of robotic and prosthetic adaptive hands, including texts (Birglen et al., 2008), recent reviews (Belter and Segil, 2013; Kragten and Herder, 2010; Pons et al., 1999) and special issues of journals (Dollar et al., 2014).

2.1. Grasp analysis for underactuated designs

Kragten and Herder (2010), noting that some of the traditional grasping metrics are not well suited to underactuated hands, define *ability to grasp* and *ability to hold*. The former addresses the ability to wrap around objects and the latter to withstand pull-out forces in various directions. These concepts can drive hand design, given a particular parameter space, which is often narrowed through the selection of desired objects/tasks and a grasp taxonomy, as outlined by Laliberté and Gosselin (1998). Other recent design work includes increasing task versatility with the selection of synergies (Gabiccini et al., 2011), improving grasp region

and load-sharing between contacts by changing joint coupling (Dollar and Howe, 2011), and investigating how finger mechanism choice affects resistance to object pull-out (Balasubramanian et al., 2012). Hammond et al. (2012) suggest systematically reducing actuated degrees of freedom by optimizing kinematics to achieve power grasps on household objects using GraspIt! (Miller and Allen, 2004).

Three-dimensional (3D) grasp analysis becomes complex, but the *ability to grasp* and *hold* can also be explored, with or without friction, using a dynamic simulation program. Keeping velocities low to minimize inertial forces, as in Aukes and Cutkosky (2013) and Aukes et al. (2014), efficient simulation tools can expand the searchable design space, making it possible to evaluate different hand configurations (e.g. three or four fingers) as well as variations in parameters such as link lengths and joint stiffness. Dynamic simulations can incorporate inertial forces or fluid dynamics. However, common challenges include numerical stability and computational efficiency during formation and breakage of many contacts with friction. The analysis in Section 4.3 uses constraint-based dynamic simulation to evaluate acquisition and the work required to pull objects in various directions.

2.2. Compliant hands for marine applications

Various underactuated manipulators have been designed specifically for marine applications. Some designs use hydraulic continuum-style fingers, which have the advantage of being neutrally buoyant and highly compliant while also providing large grasping forces. The AMADEUS sub-sea hand uses modular continuum fingers (Lane et al., 1999) with force and slip sensing. Cianchetti et al. (2011) designed an octopus-inspired hydrostat arm/manipulator. Recently, a soft hydraulic hand was deployed to collect delicate coral samples in the Red Sea with variable stiffness fingers (Galloway et al., 2016), demonstrating that compliant manipulation is a method capable of interacting with delicate sub-sea environments.

The tendon-driven Red Sea Exploratorium hand uses one motor per finger to achieve multiple grasp types for use with tools and biological specimens (Stuart et al., 2014, 2015). The elastic finger joints have low bending stiffness, and use substantial preloads to dictate finger curling behavior without diminishing grasp strength. The same principles are used in the Ocean One hands, as described in Section 3.2. In other work, Bemfica et al. (2014) demonstrate a tendon-driven hand in marine operation up to 25 m; this hand uses kinematic coupling between various joints to reduce degrees of freedom.

It should also be noted that there are many capable tendon-driven underactuated hand designs, such as those by Dollar and Howe (2010), Catalano et al. (2014), and Baril et al. (2013), that are not specifically intended for underwater operation but could potentially be adapted, with adjustments such as waterproofing the actuation system.

However, to the authors' knowledge, the Ocean One hands are the first underactuated, compliant, tendon-driven hands field-tested on a bimanual underwater robot.

2.3. Spring transmission mechanisms

Actuation is always a challenge for multi-fingered hands, and particularly for hands that will be used underwater. To reduce the distal inertia produced by hand motors, one bioinspired solution is to mount the motors on the forearm. However, this approach makes the hands less modular. Consequently, many robotic hands have the motors in the palm. Underactuated designs reduce the number of motors, often reducing overall weight and size. Backdrivability and the desire to provide transparent torque control also play a role in determining the power, mass, and number of selected actuators. Underactuation presents additional challenges involving pulleys, linkages, gears, springs, and so on, to distribute the actuation force among the fingers (Birglen et al., 2008). Designs may also use brakes or clutches to change the number of active joints and fingers (e.g. Aukes et al., 2014; Baril et al., 2013).

Among the possible solutions for distributing and modulating the forces in underactuated hands, springs are particularly attractive due to their low weight and robustness. Dechev et al. (2001) and Massa et al. (2002) use compression springs in a *spring-loaded slider*. Other implementations include a linear spring at fingertip tendon termination (Carrozza et al., 2004), a spring-loaded worm drive (Telegenov et al., 2014), helical torsion springs (Edsinger-Gonzales and Weber, 2004) or a spiral spring shaft-coupler (Chu et al., 2008). Torsional spring series-elastic actuators have also been applied to human–robot interfaces and robot joints with the advantage of impact safety (Edsinger-Gonzales and Weber, 2004; Hu et al., 2011; Kong et al., 2012; Rahman, 2012). These solutions demonstrate a variety of ways to choose, package and control torsional springs for robotic applications. In this paper, we explore the role of spring transmission stiffness in the capabilities of the Ocean One hands.

3. Overall hand design

Ocean One is intended as an avatar for humans performing exploration and manipulation tasks in deep-sea environments. The humanoid design results in two hands, located at the ends of slender arms. Accordingly, the hands should be relatively compact and light enough that they do not reduce arm payload, or affect the ‘trim’ of the platform as the arms move around. To reduce weight and to simplify cabling and control, the hands each use a single backdrivable motor housed in a pressure-compensated oil-filled chamber.¹ The motor shaft exits the oil-filled chamber through a single shaft seal, as shown in Figure 2. The remainder of the hand and transmission are wet, but covered to prevent damage from collisions, sand, and so on. The motor rotates the main

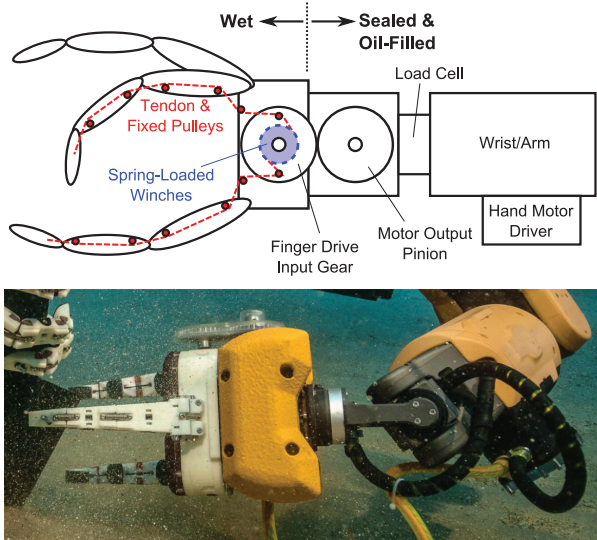


Fig. 2. Ocean One's manipulators include discrete modules. The actuator, motor driver, and load cell housings are sealed and pressure-compensated with oil-filled cavities. The hands are exposed to water, including the drive gears, transmission and tendons.

input shaft, containing spring-loaded winches for the finger tendons, through a single pair of stainless steel gears. The motor controller and other electronics are mounted on the forearm. For ease of manufacture and maintenance, the left and right hands are identical and the six fingers are interchangeable and replaceable. Additional hand component, material, and implementation details can be found in Appendix 1. For more information about the Ocean One robot, see Khatib et al. (2016).

3.1. Grasp types

The main requirements of the hand are that it should firmly grasp tools (e.g. hammers, structures) and gently extricate and grasp fragile artifacts such as pottery and glass. These requirements, coupled with a grasp taxonomy (Cutkosky, 1989; Feix et al., 2016), help determine the structure of the hand. As seen in Figure 3, three fingers – roughly analogous to the human thumb, index and fifth fingers – are selected as the minimum number to perform both parallel pinching and wrap grasping. Two of the fingers are placed at 10° skew angles (highlighted in Figure 3(b)), allowing them to pinch relatively small objects (e.g. bolts \approx 4 cm long). However, if the proximal phalanges make contact first, the fingers curl so that the fingertips pass each other to achieve a strong, interlaced wrap grasp useful for heavy tools, underwater frames or rails, and so on. The bending joints also provide some torsional compliance to help the fingers conform to irregular objects.

Figure 4 presents a schematic representation of the primary degrees of freedom and associated compliances in the hand. Each finger is a serial chain of phalanges separated

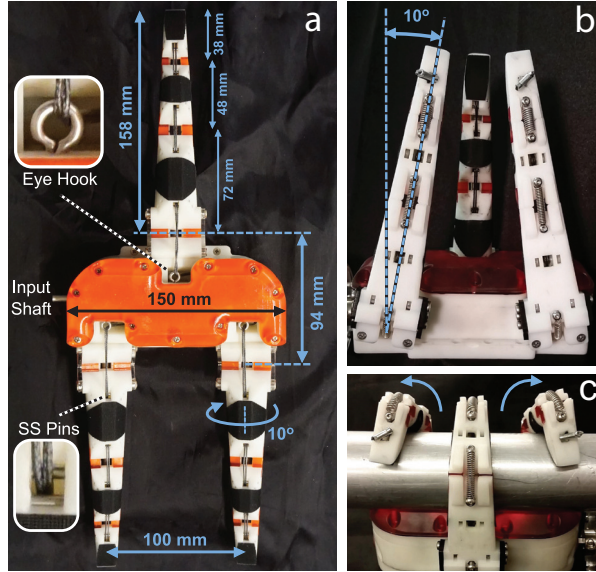


Fig. 3. The *Ocean One* hands have interchangeable fingers (a). Cables are routed over stainless steel (SS) dowel pins and eye hooks to reduce wear and friction. Slightly larger than a human hand, it accommodates a range of object sizes and grasps. Two fingers are mounted at skew angles so that the fingertips meet together for pinch grasps (b). However, if the proximal phalanges encounter a large object, the fingers wrap around it and the fingertips pass each other for an interlaced wrap grasp (c).

by joints. As found for the previously developed Red Sea Exploratorium hand (Stuart et al., 2014), the flexural joints, when actuated by the tendons and without external loads, can be approximated as pin joints with preloaded rotational springs. However, unlike pin joints, the flexures have some compliance in torsion and in lateral (adduction/abduction) bending. Among these secondary effects, the lateral bending compliance at the proximal, or base, joints is most significant for fingertip motion and is modeled using torsional springs K_{il} . The torsion springs in the transmission, along with any stretch in the tendons, are represented by K_0, K_1, K_2 .

As seen in Figure 5, the hand can perform a variety of grasps, either in precision or power configurations. In the lab, the hand is tested using objects selected primarily from the Yale–Carnegie-Mellon-University–Berkeley (YCB) object set (Calli et al., 2015). Specifically, the fingers can pinch objects (demonstrated with the AA battery, plastic water goblet, and screwdriver) or perform a wrap grasp (as shown with the large wooden block and screwdriver). The fingers conform passively to irregular object surfaces (such as the plastic pear) and a variety of object sizes. The horizontal flexibility of the joints and object shape determine the minimum pinchable object size and maximum squeeze force. For example, the rounded water goblet splayes the fingers, reducing maximum allowable pinch force, in comparison to the screwdriver. Grasps were also tested on the Ocean One platform in a swimming pool prior to field-testing; Figure 5 shows the hand pinching a plate, and grasping a PVC tube and metal mug in water.

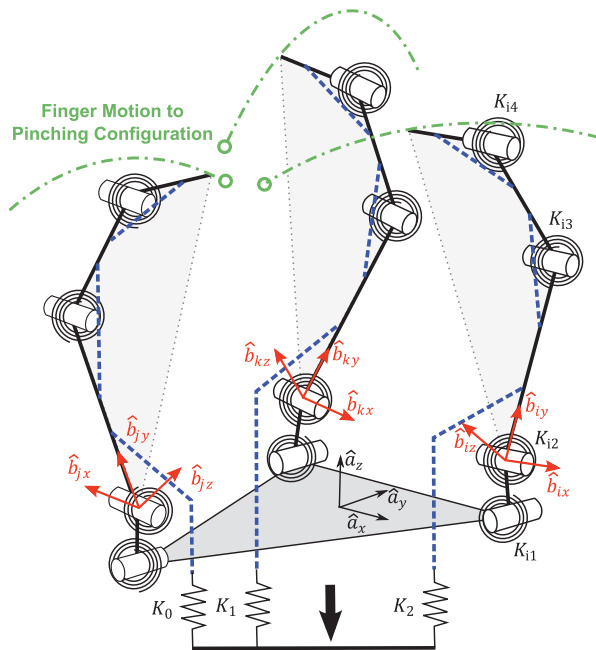


Fig. 4. Schematic of kinematics and compliance elements in the hand. Flexural joints are approximated as pin joints with preloaded torsion springs. Lateral (adduction/abduction) bending compliance is most significant for the base joints, and is represented by springs K_{il} .

3.2. Resilient tendon-driven fingers

As shown in Figure 6, the fingers are each driven by a single tendon. As in some other underactuated hands (e.g. Laliberté and Gosselin, 2001; Ciocarlie et al., 2014; Aukes et al., 2014; Stuart et al., 2014), joint stiffnesses and preloads determine the curling sequence as the hand closes, so that it will pinch small objects with straight fingers but wrap around large ones. In the Ocean One hands, the combination of robust urethane flexures and preloaded stainless steel springs allows the fingers to have a relatively low bending stiffness (which the actuator must work against whenever it closes the hand) without being floppy when the fingers are extended, due to the preload. As the joints curl, the springs change moment arm, reducing effective rotational stiffness. Each joint is split into two flexures, creating a gap in the middle, so that motion of the spring is not obstructed by the rubber. See Appendix 1 for more finger design details.

With this finger design, the proximal joint preload is selected first as the minimum value necessary to prevent sagging, uncontrollable fingers when extended. This joint should also be as soft as possible to keep grasp strength high. Similarly, the preload of the middle and distal joints should be higher than the moment necessary to close the proximal joint, in order to ensure straight-finger pinching.

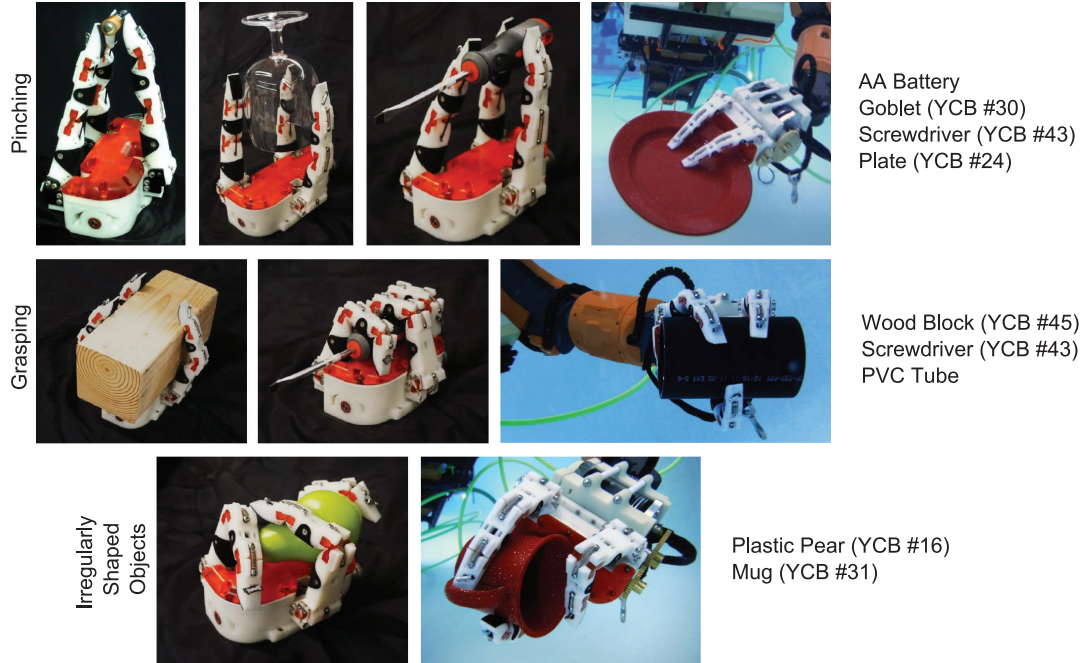


Fig. 5. The hand grasps a variety of objects from the YCB object set (Calli et al., 2015). The objects, representative of those expected in the field, are tested initially in the laboratory and subsequently in water on the *Ocean One* platform.

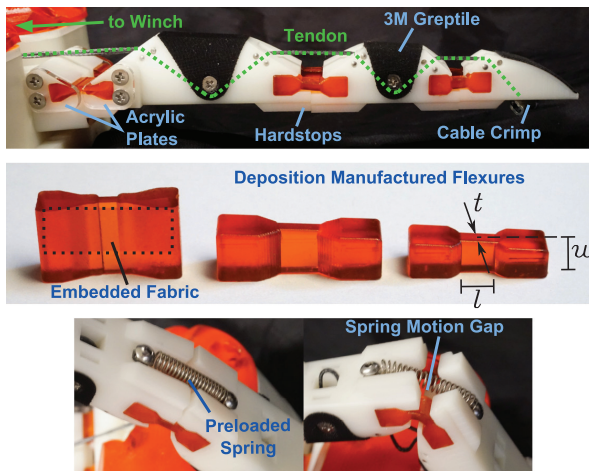


Fig. 6. Fingers are actuated using tendons that pass over polished dowel pins. Joints are made from cast urethane flexures. For additional lateral stiffness and strength, the base joints are wider and contain embedded polyester fabric. Preloaded stainless steel springs along the back sides of the joints also contribute to the joint stiffness.

The stiffness of the distal joint does not necessarily need to be as soft as the other two, as it contributes less to overall grasp strength. Finally, as in any real hand, this design method is constrained by practical geometric, material, and manufacturing limitations (e.g. there is less space to package the distal spring).

A controlled tendon tension is applied with a force gage while taking video of finger position; torque as a function

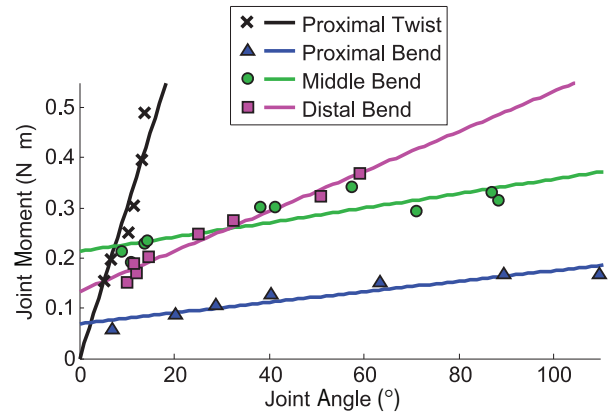


Fig. 7. Joint torques due to flexures and extension springs, as a function of bending angle. Joint preload (y -intercept) and stiffness (slope) determine finger curling behavior. Nonlinear joint moments are produced by the springs and tendons that change effective lever arm with joint angle.

of angle for each joint is shown in Figure 7. A line fit to the data, excluding points with deflections under 5° , defines the effective joint rotational stiffness (slope) and preload (y -axis intercept). We use these approximations in dynamic simulations. For comparison, the considerably higher (unactuated) torsional stiffness at the proximal joint was measured by pulling the fingertip in the \hat{b}_x direction while bent to approximately 90° . In each case, the joint stiffness is roughly constant, with some nonlinearity visible, especially for the middle joint.

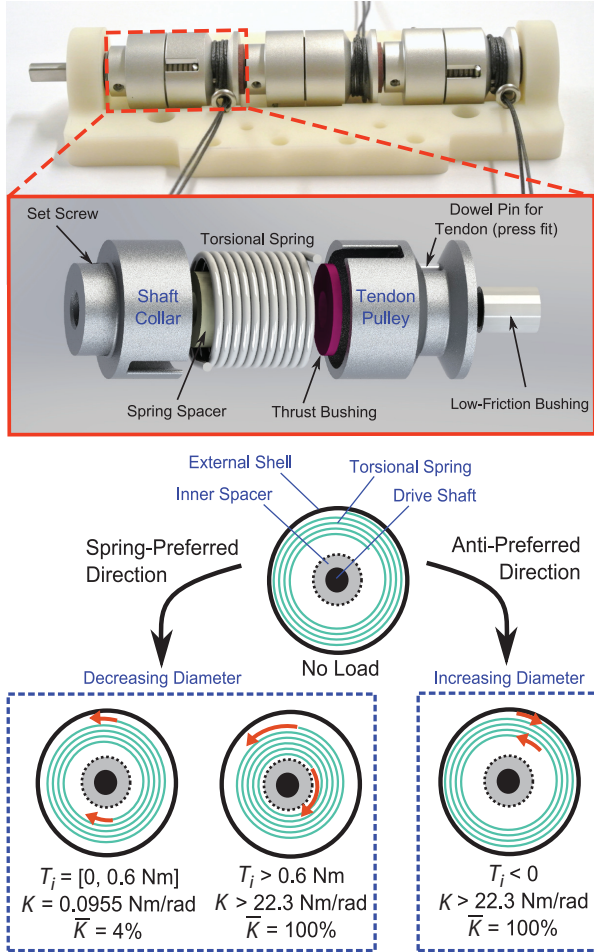


Fig. 8. Finger tendons wrap around spring-loaded winch pulleys, attached to a common drive shaft. Coil springs fit over spacers and inside coupler housings. Dimensions of spacers, springs and housings determine the effective torsional stiffness, which can be different when driven clockwise or anticlockwise, as the springs either contract against the spacers or expand against the housings.

3.3. Torsional-spring-loaded transmission

While the finger bending stiffnesses are determined largely by the desire to achieve both pinch and wrap grasps, the transmission provides an independent opportunity to tune the overall grasp stiffness. In particular, the use of coil springs that are constrained by inner and outer housings makes it possible to have a transmission with different stiffness values depending on the direction and magnitude of the applied torque.

As shown in Figure 8, a single drive shaft actuates all three fingers. Each tendon winds around its own spring-loaded winch pulley, made of two housings that engage the ends of the spring. If the spring is rotated in its normal or ‘preferred’ direction, it will initially deflect with a stiffness of 0.096 N m/rad (normalized stiffness, $\bar{K} = 4\%$) until the torque exceeds 0.6 N m , at which point the spring

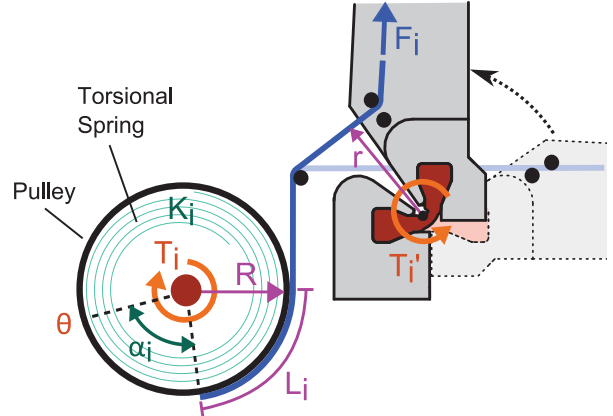


Fig. 9. Schematic of the spring-loaded winch pulley for a single finger i , showing parameters that determine tendon tension.

has wound tightly around the inner spacer and the stiffness increases to 22.3 N m/rad ($\bar{K} = 100\%$). However, if the tendon is fully unwound and the winding direction is reversed, the spring coil diameter increases and almost immediately contacts the outer wall of the housing. In this case the stiffness is consistently at its maximum value ($\bar{K} = 100\%$). The soft spring setting is useful in many situations, to promote load-sharing among the fingers. The soft setting also helps prevent damage to the hand or grasped object during accidental collisions and for this reason is selected as the default mode. However, high stiffness can be useful for applying large loads, like extricating an artifact stuck in a pile of debris, as in Section 6.

The parameters that convert shaft torque to tendon displacement and tension are illustrated in Figure 9: R is the pulley radius, and θ is the shaft rotation. The compliant rotation of a given pulley is α_i , which depends on the torsional spring constant, K_i , and tension, F_i ; the corresponding wound tendon length is L_i

$$\theta - \alpha_i = \frac{L_i}{R} \quad (1)$$

The total motor torque, τ_{motor} , is the sum of the pulley torques, so the tendon tension on each finger is given by

$$F_i = \frac{K_i (\tau_{\text{motor}} R + K_j L_j + K_k L_k - (K_j + K_k) L_i)}{R^2 (K_i + K_j + K_k)} \quad (2)$$

If $K_i = K_j = K_k$ and the stiffness becomes low, the behavior approaches that of a differential that evenly distributes actuator force to the three fingers

$$\lim_{K \rightarrow 0} F_i = \frac{1}{3} \frac{\tau_{\text{motor}}}{R} \quad (3)$$

Equation (2) is only valid when F_i is positive and the tendon is in tension. Dynamic effects, such as sudden force applied to the back of the finger, can make the tendon go slack. Also, joint twisting and lateral motion only slightly affect the tendon length, therefore transmission stiffness is primarily coupled to the closing motion of the fingers.

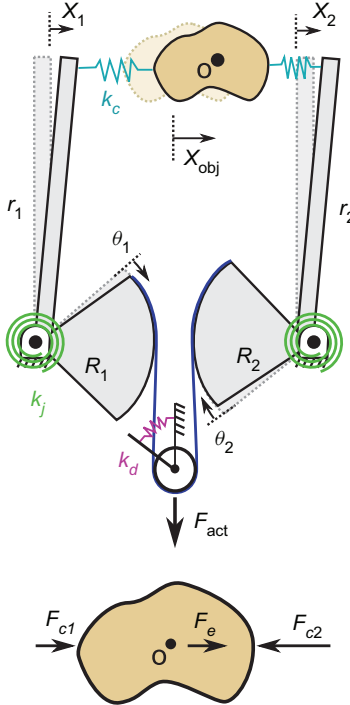


Fig. 10. Simplified planar hand includes structural compliance, represented by k_c , joint compliance, k_j , and a spring, k_d , that introduces a restoring force as a pulley differential deflects from equilibrium.

4. Grasp compliance analysis

In the previous sections we examined the elements of the hand which contribute to its performance. However, we have not addressed how to choose the stiffness values. The stiffness of the finger joints is largely constrained by the desired finger curling sequence (starting at the base and working toward the tips so that they curl around large objects and pinch small ones) and by the desire to reduce motor effort required to close the hand. The transmission stiffnesses remain to be chosen.

The compliant spring transmission affects the hand's ability to close upon irregular objects and resist external object disturbances. We start with a simplified example to introduce the main issues including internal and external grasp stiffness and the ability to resist pull-out forces. We then introduce a fast dynamic simulation tool for 3D hand and grasp modeling, including friction and compliance.

4.1. External and internal grasp stiffness

Figure 10 presents a simplified planar hand with compliance in the fingers and transmission. The contact stiffness, k_c , represents structural compliance in the fingers, tendons and fingertips. The combined effects of compliance at the joints and differential transmission are represented by k_j and k_d . In particular, k_d represents a spring that adds or subtracts from the tendon force, $F_{act}/2$, that would otherwise split

evenly between the two fingers. The stiffness k_j will most closely resemble the proximal joint stiffness, which dominates grasp behavior after object acquisition, especially in pinching.

External grasp stiffness, K_e , is defined as the scaling relationship between externally applied object force F_e and object displacement x_{obj} . To simplify algebra and make it easier to compare linear and rotational terms, let $r_1 = r_2 = R_1 = R_2 = r_{pulley} = 1$. The external grasp stiffness is then

$$K_e = \frac{2k_c(2k_d + k_j)}{k_c + 2k_d + k_j} \quad (4)$$

As $k_d \rightarrow 0$ this system represents an underactuated hand similar to the Harvard SDM ('shape deposition manufacturing') hand, which does not use extra biasing springs to set a neutral point in a pulley differential (Dollar and Howe, 2010). In this case, K_e becomes

$$K_e = \frac{2k_c k_j}{k_c + k_j} \quad (5)$$

resulting in a system where k_c and k_j act as springs in series. Typically, k_j must be chosen as a compromise to prevent the actuator from expending too much effort to close the hand, while also keeping the grasp stiff enough to hold objects precisely.

As k_d approaches infinity, $x_1 = -x_2$. This case represents compliant fingers driven by a common actuator with the same input displacement (e.g. with winch pulleys on a common shaft). The torsion springs, like those in the Ocean One hand transmission, along with tendon elasticity and structural compliance, are represented by the lumped parameter k_c . The external grasp stiffness becomes $K_e = 2k_c$, and is independent of k_j . Accordingly, the joint stiffness can be very low to reduce actuator effort without making the grasp very compliant with respect to external loads on the object.

Internal grasp stiffness, K_i , is defined as the scaling relationship between positive internal grasp force and the relative deflection of the fingertips, $\delta x = x_1 - x_2$, in the pinch direction. A high internal stiffness can be useful to prevent object pull-out which tends to force the fingers apart. If $x_{obj} = 0$, the internal grasp stiffness for this simple model becomes $k_c/2$. With a non-backdrivable actuator, soft fingers and a soft spring transmission make object pull-out significantly easier than for a stiff system.² However, with a backdrivable motor, k_c is less important, as work in forcing the fingers apart goes primarily into driving the actuator backward.

4.2. Adapting to irregular shapes

As noted in Section 2, it is accepted that softer coupling between fingers increases a hand's ability to adapt to irregular shapes, promoting gentle grasping. However, this property may have disparate effects on grasp strength and precision, depending greatly on specific object shape and

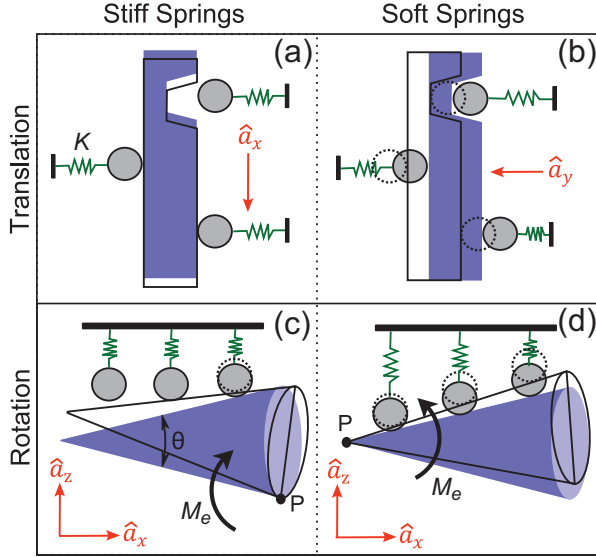


Fig. 11. Grasp effectiveness, given a transmission stiffness, is influenced by both object shape and disturbance force direction. This diagram shows *ineffective* stiffness choices. For example, the object in (a) would be held more securely if softer springs allowed one finger to get wedged in the surface feature. For the cone, a soft grasp (d) engages more fingers with the surface but external moments are better resisted with a single stiff finger engaged.

external force direction. This consideration motivates incorporating a dual-stiffness transmission in universal hands.

For example, when an object has a deep surface feature, as shown in Figure 11(a) and (b), if the pull force is in the \hat{a}_x direction it is advantageous for the finger to get wedged in the groove. This behavior engages non-active degrees of freedom in the finger, increasing pull-out work. However, if this same grasp is exposed to pull-out force in the \hat{a}_y direction (b), active degrees of freedom are engaged and the hand benefits from a stiff transmission, regardless of surface features.

Another example is shown in Figure 11(c) and (d). In (c), a hand with a softer transmission would allow more fingers to settle upon the cone farther from the pivot point, P, increasing its resistance to applied moment, $M_e\hat{a}_y$, for small deflections. On the other hand, (d) would benefit from a stiffer transmission as the farthest finger from the pivot point contacts the cone first. In human hands, the role of ulnar fingers is also observed. The fifth finger is disproportionately important when handling heavy tools, and hand surgeons sometimes replant middle digits to replace the fifth finger when it is lost (Zenn and Levin, 2005).

4.3. SimGrasp: Flexible batch simulations

Three-dimensional dynamic simulation is a useful design tool for hand analysis, especially when simulating a grasping sequence with frictional contacts, inertial or drag forces, and complex geometry. However, the simulation of multiple fingers making and breaking frictional contact with objects

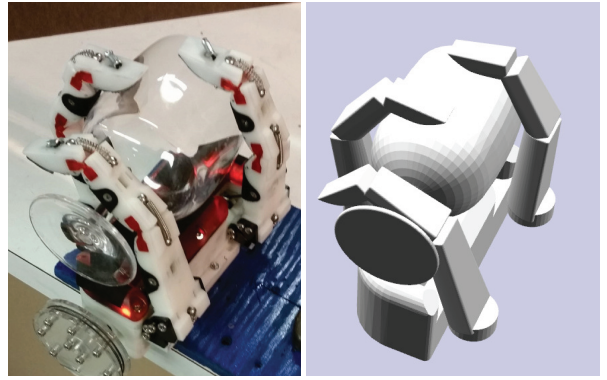


Fig. 12. SimGrasp visualization nearly matches the actual grasp of a plastic goblet (item #30 from Calli et al., 2015) with same actuation torque – natural variations in friction and object geometry produce a slightly different position for the left finger.

presents numerical challenges which have only recently been addressed by general-purpose dynamic simulation packages. SimGrasp³ is a new simulation package built upon Klamp't (Hauser, 2016), a constraint-based dynamics engine that handles large numbers of contacts efficiently. It is intended for convenient batch simulation to investigate hand design parameters. For more information, see Appendix 2.

To simulate the Ocean One hands, we approximate the kinematics as shown in Figure 4, with equivalent torsional stiffness and preload, and some joint damping and friction. As seen in Figure 12 and in the next section, the resulting simulations follow the behavior of the hand, with minor differences primarily due to variations in friction, providing useful information for evaluating changes in design parameters.

5. Transmission stiffness investigations

5.1. Hand force field

The grasp force field, calculated as a quasistatic force balance across the workspace of the hand, is a useful tool for understanding grasp behavior (Aukes et al., 2014). For each possible object location, the hand is closed upon the object with a given actuator force, and the magnitude and direction of the resultant force on the object are plotted. Without friction, the hand settles to a unique minimum energy location and the resulting vector plot also indicates the quasistatic object trajectory. With friction, this is no longer strictly true, but regions with low resultant force indicate where the object will tend to remain, unless external forces or grasping forces change significantly.

In the example in Figure 13, the static and dynamic coefficients of friction are $\mu = 0.3$ and the object is a 6.0 cm diameter cylinder. The hand closes slowly with a grasp actuation torque that ramps to 1.2 N m. The low-stiffness case, $\bar{K} = 4\%$, corresponds to the ‘normal’ torsional stiffness

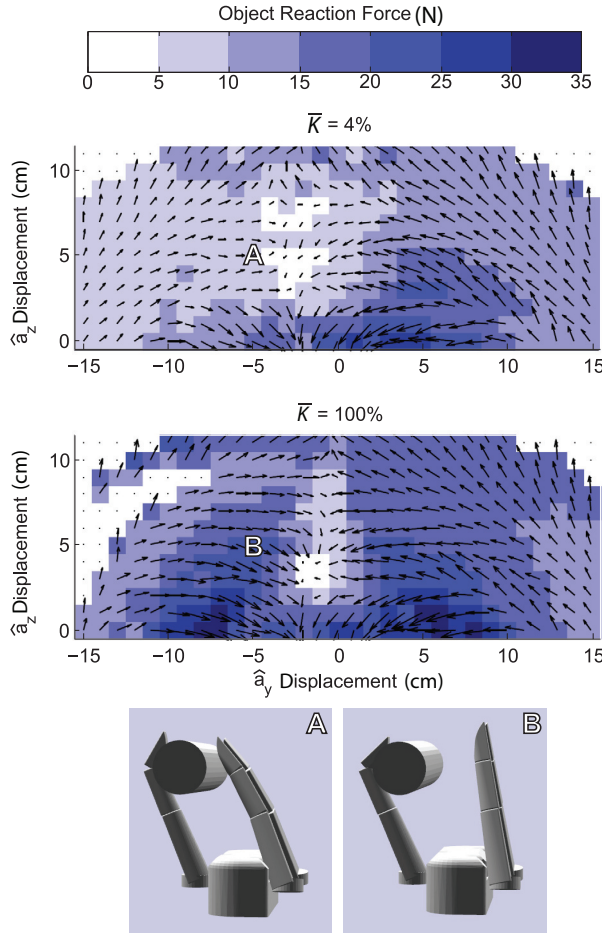


Fig. 13. Static force fields for a cylinder with typical grasping forces and different transmission stiffnesses. The softer transmission provides a larger region where the object will tend to remain, with little net force.

in the transmission, as discussed in Section 3.3; the maximum stiffness case, $\bar{K} = 100\%$, corresponds to winding the tendons in the opposite direction so that the springs immediately expand against their housings and compliance is due primarily to the fingers. We observe that the low-stiffness case has a larger region with low net force. For example, if the object is at location ‘A’ the hand will adapt to it with an off-center pinch. However, for the stiff case, if the object is at the same location, marked ‘B’, the hand will not close fully and there will be a larger net force on the object, pulling it into the hand.

5.2. Object acquisition

The acquisition region is a map of successful grasps given initial object positions and velocities relative to the hand, and is another useful metric for evaluating hands (Aukes and Cutkosky, 2013). In remotely operated underwater vehicle applications, water currents and slow response of the robot make it desirable to perform grasps promptly and reliably as soon as the hand is in a suitable position with

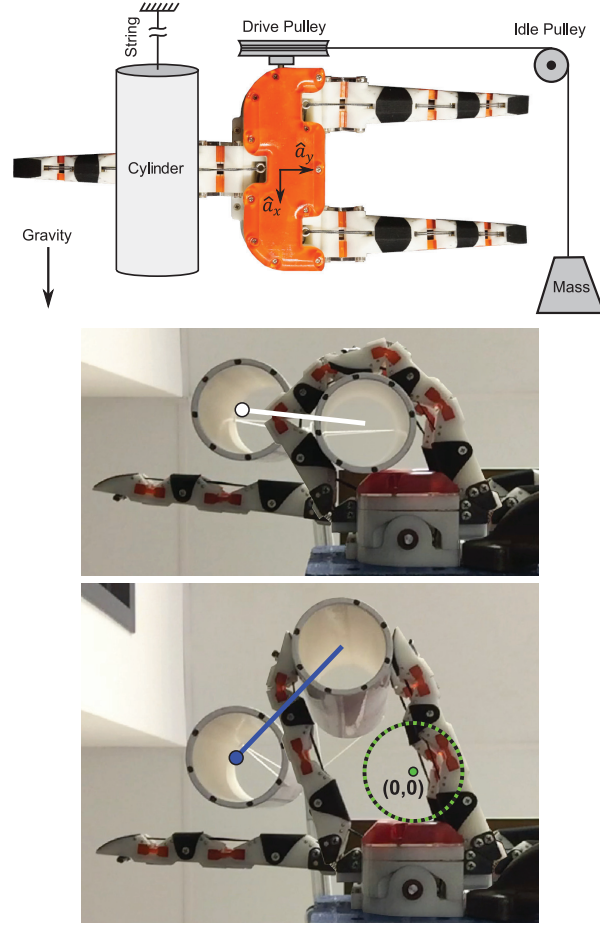


Fig. 14. To measure acquisition, a cylinder hangs from a long string at an initial location relative to the hand. The hand is closed in ≈ 1 s using a weight and pulley that apply 1 N m to the input shaft, in lieu of the motor on Ocean One. Motions are recorded with video. The white dot and line show the initial and final positions of a cylinder in a wrap grasp. The dark blue dot and line show the initial and final positions for a pinch grasp. The dotted circle shows the (0,0) coordinate location.

respect to a target. A larger acquisition region makes the hand more tolerant of positioning errors.

Controlled acquisition tests were conducted primarily to verify the accuracy of predictions by SimGrasp. The hand was mounted horizontally and a PVC tube was suspended from above in a desired initial position with respect to the palm (Figure 14). A weight and pulley system supplied torque to the input shaft, in lieu of the motor on Ocean One. As the weight is gently lowered, the hand closes upon the cylindrical object. The weight applies 1 N m of torque when at rest. Inertial forces are relatively small compared to elastic forces, but not negligible.

Figure 15 shows results for a 6 cm diameter tube with a coefficient of friction of $\mu = 0.2$. The initial and final locations of the object are denoted by dots and lines respectively. Acquisitions that result in successful wrap grasps, defined as those that bring the object to the palm, are shown in light

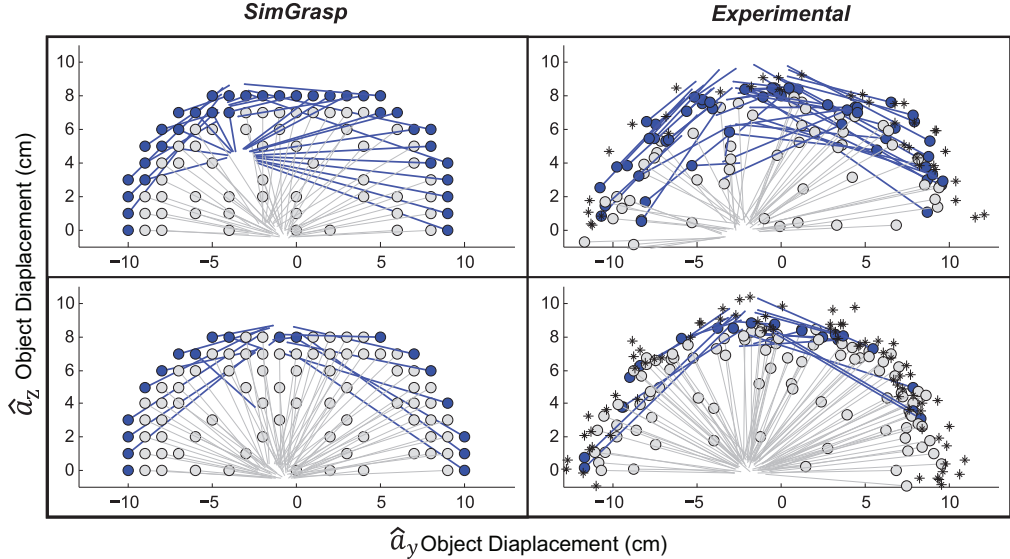


Fig. 15. Simulation and experimental acquisition regions. Light gray dots indicate object starting positions that end in a wrap grasp (with the object in contact with the palm); dark blue dots indicate starting positions that end in a pinch. Lines indicate where the object ultimately settles. Stars indicate starting positions that ended in a failed grasp.

gray, and acquisitions that result in pinch grasps are shown in dark blue. Stars indicate positions that failed to produce a grasp. The results for SimGrasp and from experiments are quite similar. The low-stiffness hand produces more pinch grasps, especially when the object is near the boundary of the acquisition region. Due to the asymmetry of one finger in opposition to two fingers, all having the same stiffness, objects tend to settle a couple of centimeters to the left of (0,0).

The experimental results, especially for the soft case, show more variability in the final object location as compared to the simulation, which is to be expected as the low-stiffness case is more sensitive to variations in friction and has a larger region with little resultant force on the object. More generally, the ability of SimGrasp to match the acquisition behavior, including some frictional and inertial effects, indicates that it can be used for evaluating variations in hand parameters. As discussed briefly in Section 7.1, future work can include different control strategies, and adding hydraulic effects for evaluating grasping underwater.

5.3. Cylinder grasp security

Resisting pull-out forces is a measure of the hand's ability to hold heavy tools or objects, and to extricate artifacts that are partially stuck in debris. The ability to securely grasp approximately cylindrical objects including tool handles and long bars was of particular concern for the Ocean One hands. The maximum pull-out force is a function of the pulling direction and therefore of the orientation of the hand with respect to the object. To test this relationship, we performed pull-out tests with a cylindrical pipe in various directions as shown in Figure 16.

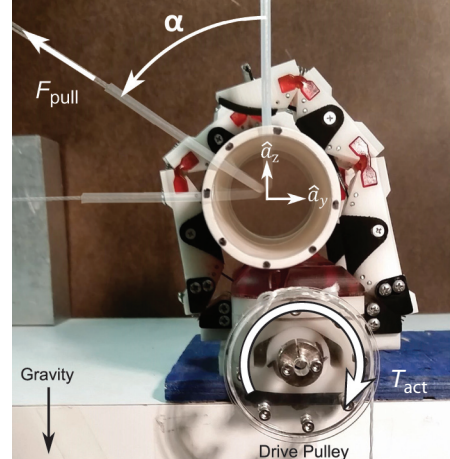


Fig. 16. A PVC tube is pulled out of the hand with varying F_{pull} orientations. As in the acquisition tests, weights and a pulley substitute for the Ocean One hand motor.

The cylinder is placed in the hand, and weights and a pulley are used to apply a grasp torque, in lieu of the Ocean One motor. A hand-held digital force gage measures the pull-out force as the object is slowly pulled out of the hand in a given direction, α . Motion is captured using video. Soft ($\bar{K} = 4\%$) and stiff ($\bar{K} = 100\%$) stiffnesses correspond to the normal and reversed transmission directions, as in the acquisition tests. An intermediate value ($\bar{K} = 21\%$) was also tested using stiffer torsional springs in the normal winding direction.

As seen in Figure 17, for the case when $\alpha = 90^\circ$, the stiff transmission unsurprisingly performs best. The simulated and empirical results agree fairly well, especially given that velocity is not controlled in these tests and there

Table 1. Work to pull out a 6 cm diameter PVC cylinder, computed for 10 cm diameter of motion ($\alpha=90^\circ$, $\mu = 0.3$, grasp torque = 1.2 N m).

\bar{K}	Experimental	Simulation
4%	2.01 J	1.86 J
21%	3.17 J	2.96 J
100%	4.07 J	3.77 J

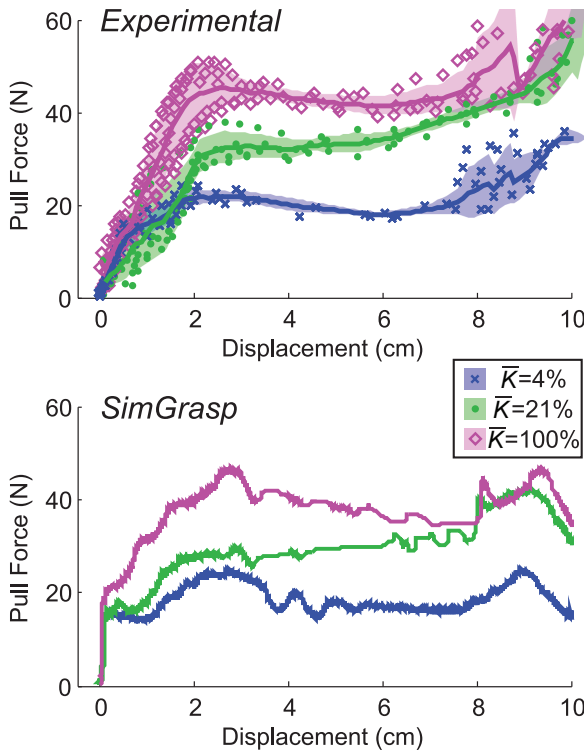


Fig. 17. Experimental and simulated pull-out results in the $\alpha = 90^\circ$ direction, for five trials each, with 1 N m actuation torque. Cylinder diameter is 6 cm, $\mu = 0.3$. Tests and simulation show improved performance with a stiff transmission. The line is the mean of the data and shaded regions show standard deviation.

are some natural variations in friction. Errors accumulate over the duration of the simulation, so differences will be higher for large displacements. A related measure of interest is the work required to pull out an object (Table 1). Here we see that the simulation slightly underestimates the required work, particularly for the low-stiffness case, which also shows the most variability at large displacements, when inertial effects and friction variations have the largest impact.

The advantage of SimGrasp lies in being able to perform batches of simulations over a range of conditions. Figure 18 shows the computed pull-out work for a range of directions, α , and stiffness values, where $\bar{K} = 100\%$ again corresponds to the maximum stiffness with the tendons wound opposite to the usual direction.

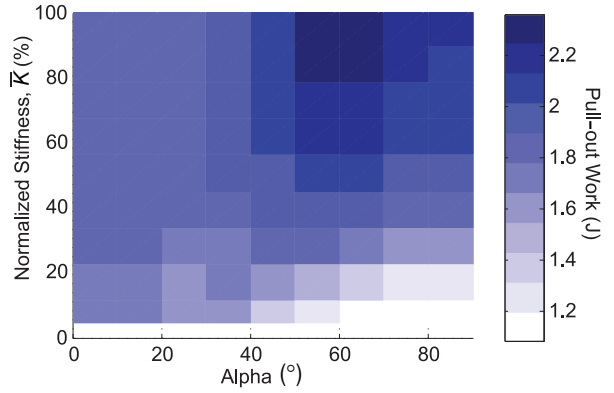


Fig. 18. Parametric study results for a 6 cm diameter plastic cylinder pulled out of the hand at various angles. As in previous pull-out examples, $\mu = 0.2$ and applied torque is 1.2 N m.

As expected, for $\alpha = 0$ transmission stiffness contributes relatively little because the actuator is backdrivable and all fingers move in an approximately symmetric way. However, at $\alpha = 90^\circ$, a stiffer transmission clearly performs better. For this particular hand design, it appears there may be an optimal pull angle of 60° with a stiff transmission, which could be considered in motion planning for the robot. However, with a soft transmission, the operator would want to pull as vertically as possible.

5.4. Task-dependent stiffness selection

Figure 19 illustrates three distinct shapes that particularly depend on the transmission stiffness, and demonstrate the importance of incorporating a dual-stiffness transmission. In case (a), which is analogous to the tapered object example considered in Figure 11(c), we observe that the soft transmission is superior, especially in the early stages when the object has rotated $< 30^\circ$. The goblet, analogous to the example in Figure 11(a), also benefits from a softer transmission that allows fingers to settle into concave features. Conversely, the block with sharp corners benefits from a stiffer transmission. The hand may settle in a slightly more advantageous configuration for this prism – small differences in contact on the block’s edges may significantly change friction and grasp strength. Along with Section 5.3, this case demonstrates that more load-sharing between fingers is not always ideal.

Although this is a limited set of objects and pull directions, they signify distinct shape features and demonstrate that performance may often monotonically improve by either softening or stiffening the transmission. Therefore, it makes sense to choose the softest and stiffest available spring rates for this dual-stiffness transmission. For the Ocean One hands, the maximum allowable spring size limits the minimum stiffness ($\bar{K} = 4\%$) while tendon compliance limits maximum stiffness ($\bar{K} = 100\%$).

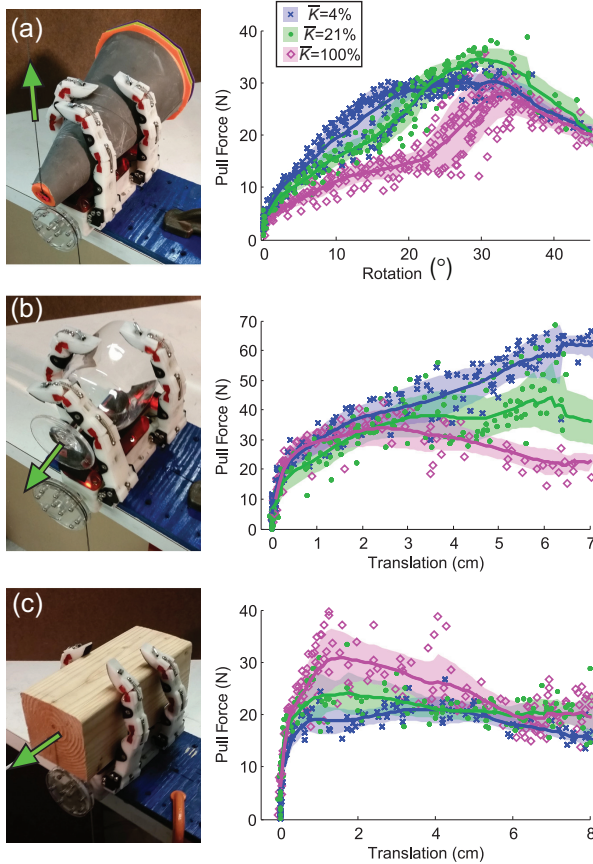


Fig. 19. Experimental pull-out results for three key objects and pull-out directions with different transmission stiffnesses. Green arrows indicate pull directions and locations: (a) applying force and moment about \hat{a}_y for a cone with $\mu = 0.7$; (b) and (c) applying force in \hat{a}_x direction for a goblet ($\mu = 0.3$) and wooden block ($\mu = 0.6$). Each case is tested for 10 pull-out trials; the line is the mean of the data and shaded regions show standard deviation.

The operator must be aware of the shape and task trends as they relate to stiffness selection in order to take advantage of the hand's best performance. Alternatively, a single intermediate stiffness could be selected that performs adequately over a range of tasks, from gentle to high strength, and requires no operator expertise; see Appendix 3 for a suggested single-stiffness design methodology. As the user interface becomes more sophisticated (addressed in Section 7.1), future work may include the estimation of optimal transmission stiffness for semi-autonomous manipulation selection. This could be achieved through a library of simulations, using a package like SimGrasp, to estimate grasp performance given predicted object shape and planned strategy.

6. Field-testing

The French ship *La Lune* sank in 1664 and now rests at a 90 m to 100 m depth, off the coast of Toulon, France.

Although discovered in 1993, this relatively well-preserved archaeological site still holds many mysteries and artifacts. During its first mission in April 2016 with DRASSM, Ocean One visited this shipwreck with the goal of extracting relics and demonstrating various other manipulation capabilities (Khatib et al., 2016).

To simplify the cognitive workload of the teleoperator during these initial trials, the hands were commanded in binary 'open' or 'close' states with buttons on the two Force Dimension™ sigma.7 haptic devices also used to control the arms and wrists. As shown in Figure 20, the robot performed bi-manual manipulation of a flexible object (a). In (b), the hands resisted internal moments and forces applied to a rigid structure between the two arms. Note that one hand is completely entwined with the box while the other is hooked with one finger; strong water currents mean the arms will not always perform an ideal grasp approach. In (c), the hand is able to resist moments due to digging with a trowel. In (d1) and (d2), the robot maneuvered into position and then picked up a ceramic artifact in a pinch while using the soft hand transmission mode.

Two dives to the *La Lune* site were conducted, and both the $\bar{K} = 4\%$ and $\bar{K} = 100\%$ transmission states were utilized to acquire a ceramic pot, shown in Figure 20(e1) to (e3). The ceramic pots were heavy and filled with silt. Gravity was in the \hat{a}_y direction relative to the hand, based on the operator's typical chosen hand orientation; results from Section 5.3 indicate that a stiff transmission could be more successful given this approach. The most successful strategy included inserting one finger inside the mouth of the vase. Although both stiffness modes were able to pick up a target object, quick motions from the robot arms or accidental impacts with the environment more easily dislodged the pots from the hand when using the $\bar{K} = 4\%$ transmission (e3) as compared to the $\bar{K} = 100\%$ transmission setting (e2). These particular vases were also covered in thick, slippery biofilm. Lateral compliance at the base joint occasionally allowed a finger to slip or push off the side of the object. This suggests that for this task an intermediate grasp actuation force would be preferred, or that the base joint should be even stiffer with respect to bending and twisting in the passive degrees of freedom. A rougher skin texture might also enhance grasp security.

As seen in Figure 21, the vase was approached from the side with the fingers oriented vertically. This operator choice is due to the kinematics and workspace of the arms and the orientation of the hand mounted on the wrist. Often if one hand was actively reaching for an object, the other hand would make contact with the ground or surrounding structures (also seen in Figure 20(d1) and (e2)), stabilizing the body from current flow disturbances. During grasp attempts, the fingers occasionally got caught on ground features and hyper-extended, severely testing the resilience of the tendons and joints – the fingers and hands survived the entire mission without maintenance. For more on design for durability, see Appendix 1.

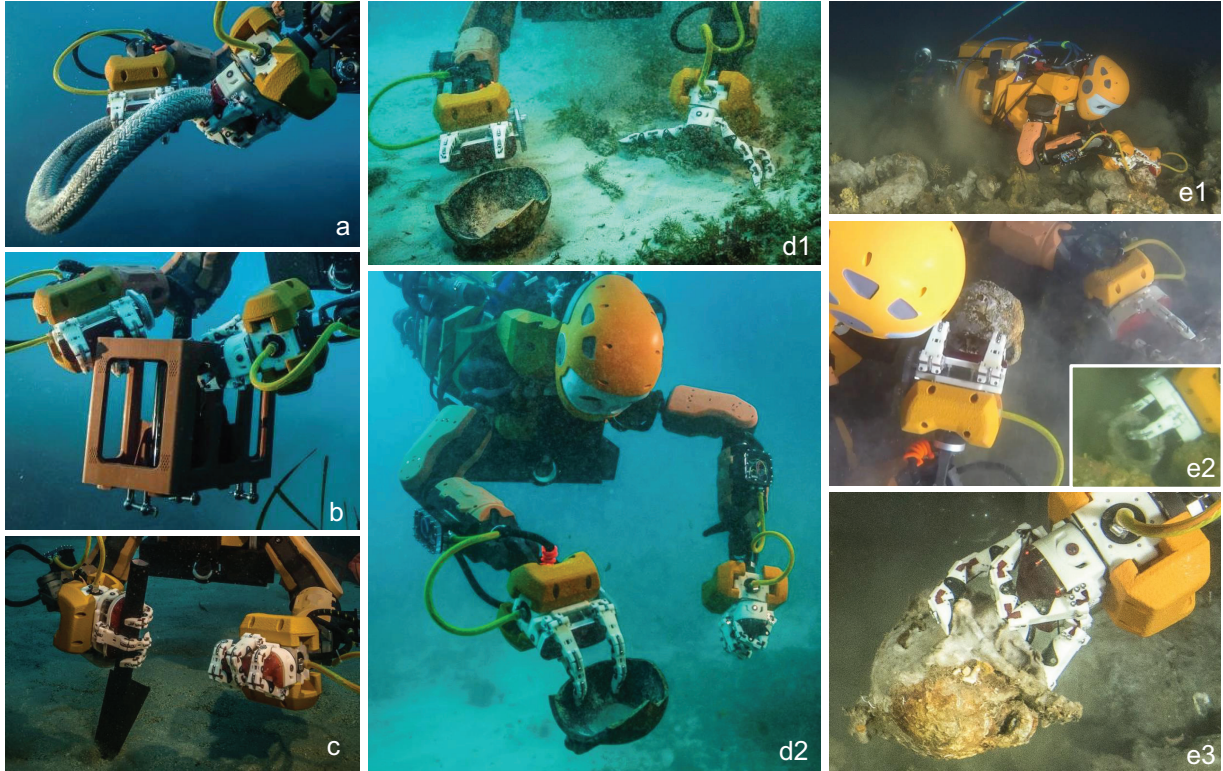


Fig. 20. The robot is able to perform reliable wrap grasps ((a) to (c)) and parallel pinching ((d1) and (d2)) during initial teleoperated manipulation trials off the southern coast of France. The robot also acquired a vase from the *La Lune* shipwreck at approximately a 91 m depth ((e1) to (e3)). Both stiff (e2) and soft (e3) transmission modes were employed. Photo credits: Frederic Osada and Teddy Seguin/DRASSM/Stanford University.

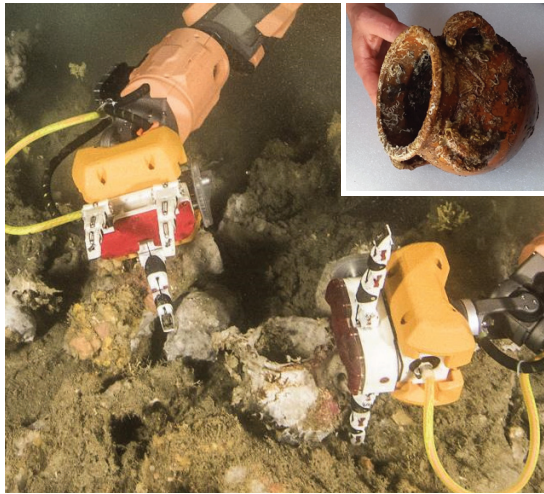


Fig. 21. During the mission to *La Lune*, the grasp was usually attempted by placing one or two fingers below the object, indicating that a stiff transmission is best for this specific task and operator. The fingers also withstood large grounding forces during object approach or when steadyng the robot against water currents. Top right: the pottery that *Ocean One* recovered from the *La Lune* after initial clearing of the biofilm. Photo credits: Frederic Osada and Teddy Seguin/DRASSM/Stanford University.

7. Conclusion

The Ocean One hand is a capable solution for deep-sea bimanual manipulation, especially when a variety of both strong and gentle pinches and grasps are required. Underactuation and compliance in the fingers and spring-loaded transmission determine grasping behavior while performing robustly, even in the harsh unstructured ocean environment. A new, geometrically constrained torsional-spring tendon winch system allows the teleoperator to select between two transmission stiffnesses by switching motor actuation direction. With this design, grasps can be precise even with very soft finger joints intended to reduce actuator effort, or loads can be shared evenly between fingers.

We find that both soft and stiff transmission modes are important for the breadth of tasks required in ocean exploration. Acquisition of free-floating cylinders is more consistent with a stiffer transmission. Yet, both object shape and pull-out direction influence how load-sharing affects grasp strength. This work can inform operators about object- and strategy-specific factors important in selecting which mode will perform best for a given task.

This is the first set of compliant, underactuated, tendon-driven hands tested on a bimanual underwater humanoid in the field. While this work validated the Ocean One hands while excavating a deep-sea archaeological site, they would

also be useful in other settings, such as subsea industrial maintenance or researching marine habitats.

7.1. Future work

The field tests of the Ocean One platform revealed many opportunities for future improvements. For example, the spring transmission design could incorporate preload and maximum throw settings, changing the behavior of the hand in different phases of grasping. Each finger could also have different behaviors, instead of being interchangeable. These factors will affect acquisition, retention, and precision of the hand, and represent a more complete set of design parameters worth exploring further. As noted in Section 5.2, it would be useful to extend SimGrasp to include the effects of water when simulating object acquisition operations.

More sophisticated semi-autonomous control strategies and combined visual/haptic feedback have the potential to significantly improve the operators' skill in underwater tasks. In addition, while the hands are equipped with force/torque sensors at the wrist, they have no tactile sensing at the fingertips. This information would enhance the sense of presence and dexterity for manipulation tasks. Special considerations will be needed to address large changes in ambient pressure and waterproofing for the harsh ocean environment.

Acknowledgements

The authors acknowledge the work of Xiyang Yeh, Brian Soe, Shameek Ganguly, Bo Kim, Gerald Brantner, and the Meka Robotics team, including Aaron Edsinger and Mitchell Barham, for their dedication in building the Ocean One robot. Vincent Creuze and Michel L'Hour, as well as the rest of the DRASSM crew, helped make the mission to the *La Lune* shipwreck possible. We thank the current and previous members of the Biomimetic and Dexterous Manipulation Lab for their support, particularly Daniel Aukes.

Funding

The author(s) disclosed receipt of the following financial support for the research, authorship, and/or publication of this article: This project was supported by King Abdullah University of Science and Technology's Red Sea Robotic Exploratorium grant (Stanford agreement number SPO 103760). H Stuart was supported by the NSF Graduate Research Fellowship (grant number DGE-114747) and the Stanford Graduate Fellowship Program. Any opinions, findings, conclusions or recommendations expressed in this material are those of the authors and do not necessarily reflect the views of the funding sources.

Notes

1. The actuator housing is also covered in orange flotation foam to compensate partially for changes in the robot's center of mass as the arms move.
2. For example, the hands on RoboSimian used a non-backdrivable transmission and relatively stiff fingers so that it

could support its entire weight hanging from one hand (Hebert et al., 2015).

3. <https://bitbucket.org/shiquan/sim-grasp>

References

- Aukes DM and Cutkosky MR (2013) Simulation-based tools for evaluating underactuated hand designs. In: *2013 IEEE international conference on robotics and automation (ICRA)*, Karlsruhe, Germany, 6–10 May 2013, pp.2067–2073. Piscataway, NJ: IEEE Press.
- Aukes DM, Heyneman B, Ulmen J, et al. (2014) Design and testing of a selectively compliant underactuated hand. *The International Journal of Robotics Research* 33(5): 721–735.
- Balasubramanian R, Belter JT and Dollar AM (2012) Disturbance response of two-link underactuated serial-link chains. *Journal of Mechanisms and Robotics* 4(2): 021013.
- Baril M, Laliberté T, Gosselin C, et al. (2013) On the design of a mechanically programmable underactuated anthropomorphic prosthetic gripper. *ASME Journal of Mechanical Design* 135(12): 121008.
- Belter JT and Segil JL (2013) Mechanical design and performance specifications of anthropomorphic prosthetic hands: A review. *Journal of Rehabilitation Research and Development* 50(5): 599–618.
- Bemfica JR, Melchiorri C, Moriello L, et al. (2014) A three-fingered cable-driven gripper for underwater applications. In: *2014 IEEE international conference on robotics and automation (ICRA)*, Hong Kong, China, 31 May–7 June 2014, pp.2469–2474. Piscataway, NJ: IEEE Press.
- Birglen L, Laliberté T and Gosselin C (2008) *Underactuated Robotic Hands* (*Springer Tracts in Advanced Robotics*, vol. 40). Berlin/Heidelberg: Springer.
- Calli B, Walsman A, Singh A, et al. (2015) Benchmarking in manipulation research: Using the Yale-CMU-Berkeley object and model set. *IEEE Robotics and Automation Magazine* 22(3): 36–52.
- Carrozza MC, Suppo C, Sebastiani F, et al. (2004) The SPRING hand: Development of a self-adaptive prosthesis for restoring natural grasping. *Autonomous Robots* 16(2): 125–141.
- Catalano MG, Grioli G, Farnioli E, et al. (2014) Adaptive synergies for the design and control of the Pisa/IIT SoftHand. *The International Journal of Robotics Research* 33(5): 768–782.
- Chu Ju, Jung D and Lee Y (2008) Design and control of a multifunction myoelectric hand with new adaptive grasping and self-locking mechanisms. In: *2008 IEEE international conference on robotics and automation*, Pasadena, USA, 19–23 May 2008, pp.743–748. Piscataway, NJ: IEEE Press.
- Cianchetti M, Arienti A, Follador M, et al. (2011) Design concept and validation of a robotic arm inspired by the octopus. *Materials Science and Engineering C* 31(6): 1230–1239.
- Ciocarlie M, Hicks FM, Holmberg R, et al. (2014) The Velo gripper: A versatile single-actuator design for enveloping, parallel and fingertip grasps. *The International Journal of Robotics Research* 33(5): 753–767.
- Cutkosky M (1989) On grasp choice, grasp models, and the design of hands for manufacturing tasks. *IEEE Transactions on Robotics and Automation* 5(3): 269–279.
- Dechev N, Cleghorn W and Naumann S (2001) Multiple finger, passive adaptive grasp prosthetic hand. *Mechanism and Machine Theory* 36(10): 1157–1173.

- Dollar AM and Howe RD (2010) The highly adaptive SDM hand: Design and performance evaluation. *The International Journal of Robotics Research* 29(5): 585–597.
- Dollar AM and Howe RD (2011) Joint coupling design of underactuated hands for unstructured environments. *The International Journal of Robotics Research* 30(9): 1157–1169.
- Dollar AM, Bicchi A, Cutkosky MR, et al. (2014) Special issue on the mechanics and design of robotic hands. *The International Journal of Robotics Research* 33(5): 675–676.
- Edsinger-Gonzales A and Weber J (2004) Domo: A force sensing humanoid robot for manipulation research. In: *2004 4th IEEE/RAS international conference on humanoid robots*, Santa Monica, USA, 10–12 November 2004, pp.273–291. Piscataway, NJ: IEEE Press.
- Feix T, Romero J, Schmiedmayer HB, et al. (2016) The grasp taxonomy of human grasp types. *IEEE Transactions on Human-Machine Systems* 46(1): 66–77.
- Gabiccini M, Bicchi A, Prattichizzo D, et al. (2011) On the role of hand synergies in the optimal choice of grasping forces. *Autonomous Robots* 31(2–3): 235–252.
- Galloway KC, Becker KP, Phillips B, et al. (2016) Soft robotic grippers for biological sampling on deep reefs. *Soft Robotics* 3(1): 23–33.
- Hammond FL, Weisz J, de la Llera Kurth AA, et al. (2012) Towards a design optimization method for reducing the mechanical complexity of underactuated robotic hands. In: *2012 IEEE international conference on robotics and automation*, Minnesota, USA, 14–18 May 2012, pp.2843–2850. Piscataway, NJ: IEEE Press.
- Hauser K (2016) *Robust Contact Generation for Robot Simulation with Unstructured Meshes*. Cham, Switzerland: Springer International Publishing, pp.357–373.
- Hebert P, Bajracharya M, Ma J, et al. (2015) Mobile manipulation and mobility as manipulation-design and algorithms of RoboSimian. *Journal of Field Robotics* 32(2): 255–274.
- Hu J, Edsinger A, Lim YJ, et al. (2011) An advanced medical robotic system augmenting healthcare capabilities – Robotic nursing assistant. In: *2011 IEEE international conference on robotics and automation (ICRA)*, Shanghai, China, 9–13 May 2011, pp.6264–6269. Piscataway, NJ: IEEE Press.
- Johnson M, Shrewsbury B, Bertrand S, et al. (2015) Team IHMC's lessons learned from the DARPA robotics challenge trials. *Journal of Field Robotics* 32(2): 192–208.
- Karumanchi S, Edelberg K, Baldwin I, et al. (2016) Team RoboSimian: Semi-autonomous mobile manipulation at the 2015 DARPA robotics challenge finals. *Journal of Field Robotics: Special Issue on the 2015 DRC Finals* 00(00): 1–28.
- Khatib O, Yeh X, Brantner G, et al. (2016) Ocean One: A Robotic Avatar for Oceanic Discovery. *IEEE Robotics & Automation Magazine* 23(4): 20–29.
- Kong K, Bae J, Member S, et al. (2012) A compact rotary series elastic actuator for human assistive systems. *IEEE/ASME Transactions on Mechatronics* 17(2): 288–297.
- Kragten GA and Herder JL (2010) The ability of underactuated hands to grasp and hold objects. *Mechanism and Machine Theory* 45(3): 408–425.
- Laliberté T and Gosselin CM (1998) Simulation and design of underactuated mechanical hands. *Mechanism and Machine Theory* 33(1–2): 39–57.
- Laliberté T and Gosselin CM (2001) Underactuation in space robotic hands. In: *Proceedings of the 6th international symposium on artificial intelligence and robotics & automation in space: i-SAIRAS*, Montréal, Canada, 18–22 June 2001, pp.1–8. Québec: Canadian Space Agency.
- Lane D, Davies J, Robinson G, et al. (1999) The AMADEUS dexterous subsea hand: Design, modeling, and sensor processing. *IEEE Journal of Oceanic Engineering* 24(1): 96–111.
- Ma RR, Belter JT and Dollar AM (2015) Hybrid deposition manufacturing: Design strategies for multimaterial mechanisms via three-dimensional printing and material deposition. *Journal of Mechanisms and Robotics* 7(2): 021002.
- Massa B, Roccella S, Carrozza M, et al. (2002) Design and development of an underactuated prosthetic hand. In: *Proceedings of the 2002 IEEE international conference on robotics and automation*, Washington, DC, 11–15 May 2002, pp.3374–3379. Piscataway, NJ: IEEE Press.
- Miller AT and Allen PK (2004) Graspit! A versatile simulator for robotic grasping. *IEEE Robotics & Automation Magazine* 11(4): 110–122.
- Pons J, Ceres R and Pfeiffer F (1999) Multifingered dexterous robotics hand design and control: A review. *Robotica* 17(06): 661–674.
- Pringle A (1919) *Artificial hand*. Patent US1324564 A, USA.
- Rahman SMM (2012) A novel variable impedance compact compliant series elastic actuator for human-friendly soft robotics applications. In: *2012 IEEE RO-MAN: The 21st IEEE international symposium on robot and human interactive communication*, Paris, France, 9–12 September 2012, pp.19–24. Piscataway, NJ: IEEE Press.
- Stuart HS, Bagheri M, Wang S, et al. (2015) Suction helps in a pinch: Improving underwater manipulation with gentle suction flow. In: *2015 IEEE/RSJ international conference on intelligent robots and systems (IROS)*, Hamburg, Germany, 28 September–2 October 2015, pp.2279–2284. Piscataway, NJ: IEEE Press.
- Stuart HS, Wang S, Gardineer B, et al. (2014) A compliant underactuated hand with suction flow for underwater mobile manipulation. In: *2014 IEEE international conference on robotics and automation (ICRA)*, Hong Kong, China, 31 May–7 June 2014, pp.6691–6697. Piscataway, NJ: IEEE Press.
- Telegenov K, Tlegénov Y and Shintemirov A (2014) An underactuated adaptive 3D printed robotic gripper. In: *2014 10th France-Japan/8th Europe-Asia congress on Mecatronics (MECATRONICS)*, Tokyo, Japan, 27–30 November 2014, pp.110–115. Piscataway, NJ: IEEE Press.
- Zenn MR and Levin S (2005) Multiple digit replantation. In: Weinzweig N and Weinzweig J (eds) *The Mutilated Hand*. Philadelphia, PA: Elsevier, pp.217–224.

Appendix 1 Component and material details

Each Ocean One hand is driven by a Maxon EC-45 70 W motor. In comparison to some other hands, the transmission is backdrivable with a 32:1 overall speed ratio. Hence, overload forces at the fingers can be absorbed by backdriving the motor, as well as in the elastic transmission. This also allows for better torque transparency when controlling the hands.

The hand assembly, shown in Figure 3, has a mass of 0.8 kg and a weight of 2.5 N in seawater at atmospheric pressure. The phalanges and palm are fabricated primarily

from 3D-printed Accura Xtreme 200™ plastic, with properties similar to stiff polypropylene or ABS (acrylonitrile-butadiene-styrene). This is an ultraviolet-cured material and is therefore susceptible to aging with sun exposure and most suitable for short-term prototypes. Future versions of the hand may employ protective coating or electroless plating to prevent deterioration of 3D printed parts. The palm is covered with a 12 mm thick deformable Smooth-On Vytaflex 20™ urethane pad to increase contact compliance and friction. Additionally, contact surfaces of the fingers are covered in textured black 3M Greptile™ skin with adhesive backing to provide minor additional padding and to increase friction.

Each of the fingers' joints is composed of flexible urethane (Smooth-On PMC 780™, Shore A 80). For maximum strength, they are cast machined wax molds and then glued into place. This approach produces a very smooth surface finish, which resists tearing and fatigue better than flexures which are either 3D printed from soft material or cast directly into cavities in 3D printed parts (e.g. Stuart et al., 2014; Ma et al., 2015). For additional lateral stiffness and strength, the proximal flexures contain an embedded polyester fabric along the neutral axis and acrylic side plates to prevent lateral deflection. Preloaded stainless steel springs run along the backsides of the joints to provide additional finger extension, especially when the fingers are open. Joint geometry, stiffness, and preloads are summarized in Table 2.

Joint ranges of motion are 110°, 120° and 100° for the proximal, medial and distal joints, respectively. The tendons are made from 1 mm diameter Dyneema™ fishing line rated at 550 N. For additional strength, the tendons are doubled, looping around pins on the transmission winch pulleys and terminating with a crimp at the fingertip (Figure 6). In light of observed problems with tendon failures at the recent Defense Advanced Research Projects Agency (DARPA) Robotics Challenge (Johnson et al., 2015; Karumanchi et al., 2016), these tendons are intentionally over-designed, because tendon failure at depth would compromise the entire mission. To reduce wear and friction, the tendons pass over polished dowel pins wherever there is a change in direction, as highlighted in Figure 3(a).

The tendon torsional spring-winches are machined out of aluminum and hard-anodized while the springs and other hardware are stainless steel. Silicone grease and thrust bushings are used to reduce friction at sliding interfaces. The housings are sized for a soft 0.096 N m/rad spring, allowing up to 360° rotation. The winch-pulley has an 8 mm radius, yielding a total tendon compliant extension of 5 cm and a hand capable of load-sharing between fingers. At 1 N m of shaft torque (a typical power grasp), the three springs will each rotate to about 190°.

Appendix 2 SimGrasp

SimGrasp simplifies the process of hand definition, including the control strategy, providing a framework for

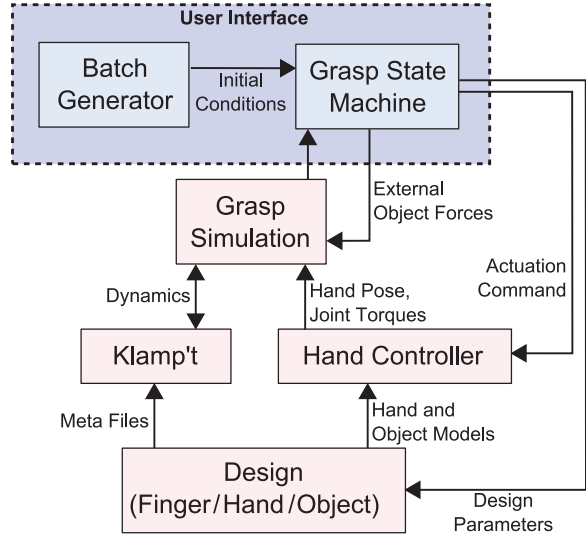


Fig. 22. Diagram describing workflow of SimGrasp batch simulations. The user interfaces with the blue module, which includes the ‘Batch Generator’ and ‘Grasp State Machine’ for defining the grasp metrics, design parameters, and hand control strategies.

implementing complex grasping sequences and batch simulation over a range of design parameters. As laid out in Figure 22, SimGrasp is composed of five modules that interface with Klamp’t (Hauser, 2016). The batch generator changes and tracks sequential initial conditions and sets design parameters for each simulation trial. It passes these values to the grasp state machine which handles the high-level control and actuation commands given various possible states of the grasp, for example ‘grasping’ or ‘pull out’. The hand and object design parameters, which include geometry, joint orientations and mass, are passed to the design module which generates the necessary XML files and geometric models of the system.

The hand controller interprets high-level actuation commands and tracks hand pose while the grasp simulation module interfaces with both the hand controller and Klamp’t. The user need only edit the batch generator and grasp state machine in order to develop a set of dynamic simulations to investigate a range of design parameters of interest.

Appendix 3 Selecting a single stiffness

Table 3 compares the displacements and relative amounts of work required to pull an object in each case in Figure 19, normalized to the best case for each task.

It is possible that for some spring transmission designs a single stiffness must be selected for all tasks. If this is the case, we can let C_w be a weighting factor for pull-out work and C_σ be a weighting factor that penalizes variability in results over repeated trials. We can construct a simple cost function based on the normalized work, w , and variation, σ , as

$$P = C_w \cdot w + C_\sigma (1 - \sqrt{2}\sigma) \quad (6)$$

Table 2. Finger joint component stiffness and geometric parameters. The tendon radius changes throughout range of motion and is estimated given a fixed center of rotation. The proximal twist joint is modeled as independent of joint pose.

	Proximal twist	Proximal bend	Medial bend	Distal bend
Joint Range	Approx. $\pm 10^\circ$	0° to 110°	0° to 120°	0° to 100°
Rotational Stiffness	30.0 N mm°	1.1 N mm°	1.4 N mm°	4.0 N mm°
Rotational Preload	0 N mm	69.7 N mm	213.1 N mm	133.5 N mm
Tendon Radius	—	9.2 mm to 19.9 mm	6.6 mm to 15.4 mm	4.6 mm to 8.2 mm
Flexure ($t \times l \times w$)	—	$1.8 \times 2.8 \times 12.0 \text{ mm}$	$3.0 \times 6.0 \times 7.4 \text{ mm}$	$3.5 \times 5.0 \times 5.2 \text{ mm}$
Extension Spring Stiffness	—	1.0 N/mm	1.5 N/mm	1.9 N/mm

Table 3. Normalized work for the three cases, found by integrating force to the maximum allowable displacement of the object in the hand. Friction coefficient is measured between the object and the fingerpad material.

	Task A	Task B	Task C
Friction coefficient	0.7	0.3	0.6
Maximum displacement	30°	4 cm	2 cm
$\bar{K}=4\%$	1.00	1.00	0.65
$\bar{K}=21\%$	0.92	0.86	0.83
$\bar{K}=100\%$	0.59	0.85	1.00

where

$$C_\sigma = 1 - C_w, C_w = [0, 1] \quad (7)$$

Figure 23 compares the normalized work and variability for the trials in Figure 19. Interestingly, the intermediate stiffness is preferable to either the softest or stiffest cases over most values of C_w to satisfy this set of tasks. This indicates that for many combinations of tasks a middle stiffness may be the best choice to produce a generally well-performing hand, resistant to pull-out disturbances. It also contradicts the current trend to make all fingers as load-sharing as possible.

It is not feasible to test a large set of tasks experimentally. Future work includes simulating a library of tasks using a

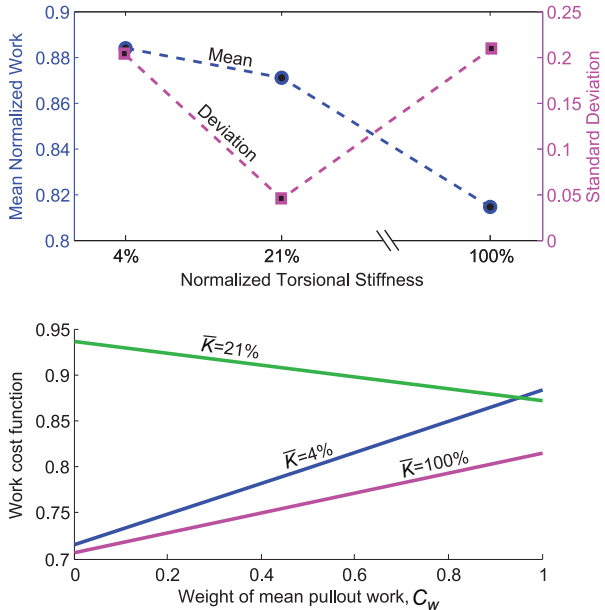


Fig. 23. Normalized work and standard deviation of pull-out given various transmission stiffnesses for the set of three tasks. A cost function indicates that the intermediate stiffness is a good choice for consistent performance.

dynamic tool such as SimGrasp in order to select a stiffness that best satisfies an arbitrary application.